Available online at www.sciencedirect.com
SCIENCE DIRECT®
Journal of Catalysis 221 (2004) 241–251
JOURNAL OF CATALYSIS
www.elsevier.com/locate/jcat

Alkane hydrocracking: shape selectivity or kinetics?

Theo L.M. Maesen,[b,*] Sofia Calero,[a] Merijn Schenk,[a] and Berend Smit [a]

[a] *Department of Chemical Engineering, University of Amsterdam, Nieuwe Achtergracht 166, 1018 WV, Amsterdam, The Netherlands*
[b] *ChevronTexaco, Energy Technology Company, 100 Chevron Way, Richmond, CA 94802-0627, USA*

Received 21 May 2003; revised 23 July 2003; accepted 24 July 2003

Abstract

A critical evaluation of published alkane hydrocracking product distributions shows that the kinetic network shifts from predominantly $\alpha\alpha\gamma$-trimethylalkane to predominantly $\alpha\alpha$- and $\alpha\gamma$-dimethylalkane hydrocracking when the acid sites are insufficiently covered with alkenes. Since $\alpha\alpha\gamma$-trimethylalkane hydrocracking has a higher symmetry than $\alpha\alpha$- and $\alpha\gamma$-dimethylalkane hydrocracking, this alteration in the predominant hydrocracking pathway changes the product distribution from a histogram with a single sharp maximum irrespective of the alkane length to histograms with several maxima depending on the feed alkane length. Thermodynamic, kinetic, and mechanistic considerations are presented to explain both types of histograms in great detail. These largely kinetic explanations supplant earlier attempts at linking the features of the hydrocracking product distributions to features of the topologies of the various (zeolite-based) catalysts employed.
© 2003 Elsevier Inc. All rights reserved.

Keywords: Amorphous aluminosilicates; MOR-, FAU-, EMT-, BEA-type zeolites; Alkane hydrocracking; Kinetics

1. Introduction

Alkane (hydro)conversion has been extensively studied due to its importance in the refinery and petrochemical processes of FCC [1,2], hydrocracking [1–4], light naphtha hydroisomerization [2,5], and hydrodewaxing [6,7]. Zeolites play an important role in the catalysts used in these processes because they improve catalytic activity, selectivity, or stability by imparting shape selectivity [1–7].

Shape selectivity is best described as the unambiguous effect of zeolite pore topology on catalytic selectivity [8]. As part of an effort to gain a fundamental understanding of shape selectivity we have employed molecular simulations to elucidate the relevant processes at a molecular level [9–13]. Research so far suggests that the fate of a molecule depends on its Gibbs free energy of adsorption and the relative heights of the Gibbs free energy barriers to adsorption, reaction, diffusion, and desorption [11]. Transition-state shape selectivity occurs when the zeolite topology affects the fate of an adsorbed molecule by modifying the Gibbs free energy barriers to reaction [14,15]. When the mass transfer rate between the gas phase and the adsorbed phase limits the reaction rate, four additional forms of shape selectivity can occur:

1. Zeolites preferentially consume molecules that combine a low Gibbs free energy of adsorption with a low Gibbs free energy barrier to diffusion (reactant shape selectivity [16]);
2. Zeolites preferentially yield molecules that combine a high Gibbs free energy of adsorption with a low Gibbs free energy barrier to diffusion (product shape selectivity [16]) [11];
3. Zeolites preferentially form reaction intermediates that combine a low Gibbs free energy of adsorption (and formation in the adsorbed phase) with a high Gibbs free energy barrier to diffusion (reaction intermediate shape selectivity) [10,11];
4. Zeolites preferentially process reactants at exterior surface pockets or pore mouths if they exhibit too high a Gibbs free energy of adsorption [17] or too high a Gibbs free energy barrier to diffusion [18–20] to fully penetrate the adsorbate (in so far as this phenomenon is indeed shape selectivity (as in [17]) it goes by a plethora of names [8]).

If only adsorbate-adsorbent interactions are considered, the Gibbs free energy of adsorption is determined by the site

* Corresponding author.
E-mail address: tmaesen@chevrontexaco.com (T.L.M. Maesen).

0021-9517/$ – see front matter © 2003 Elsevier Inc. All rights reserved.
doi:10.1016/j.jcat.2003.07.003

where the shape of the adsorbent and the adsorbate topology are the most commensurate; the Gibbs free energy barrier to diffusion is determined by the site where they are the least commensurate [11]. In addition to adsorbate-adsorbent interactions intermolecular interactions among reactants, intermediates, and products affect the Gibbs free energy of adsorption [12,13] and the Gibbs free energy barriers to adsorption, diffusion, and desorption [12,13,18].

A reported change in *n*-alkane hydrocracking shape selectivity of FAU-type zeolites following a decrease in both the acid site density and the effective crystal size [21] as a result of a steaming procedure [22,23] provided the initial motivation for the current study. The change of selectivity with acid site density and effective crystal size suggested that FAU-type zeolites exhibit a form of mass-transfer shape selectivity in *n*-heptadecane (*n*-C_{17}) hydroconversion, preferentially forming and hydrocracking particular alkane isomers at the expense of others [22–24]. However, molecular simulations [11–13] corroborate experimental data [25] that show no evidence for the preferential formation of particular alkane isomers. Isomers with the same degree of branching tend to have similar Gibbs free energies of adsorption and formation in FAU-type zeolites [11,13,25]. The FAU-type windows separating the FAU-type supercages [26] are too large to pose a significant Gibbs free energy barrier to diffusion. Accordingly, molecular simulations suggest that the FAU-type topology induces neither the preferential formation nor the preferential desorption of any particular alkane isomer. This strongly suggests that FAU-type zeolites do not exhibit any form of mass-transfer shape selectivity in *n*-alkane hydrocracking. Here we show that the most likely cause for the change of *n*-C_{17} hydrocracking selectivity with acid site density and crystal size [22,23] is not due to shape selectivity, but to a change in alkene coverage of the acid sites not related to the zeolite topology.

First we will discuss the traditional *n*-alkane hydrocracking mechanism, and establish that the fraction of *i*-alkanes in the hydrocracking product slate of large pore catalysts is a measure for the extent of $\alpha\alpha\gamma$-trimethylalkene hydrocracking as opposed to $\alpha\alpha$- and $\alpha\gamma$-dimethylalkene hydrocracking, and—therefore—for the extent of coverage of the acid sites with alkenes. Subsequently we will discuss changes to the hydrocracking product slate that occur when the alkene coverage decreases. Initially the focus is on *n*-decane (*n*-C_{10}) hydroconversion, because the majority of published catalytic data involve Pt-loaded-zeolite-catalyzed decane (C_{10}) hydroconversion, and because C_{10} is the longest alkane for which the gas-phase thermodynamic data of all relevant isomers are readily available [27]. From C_{10} we extrapolate to the hydroconversion of longer *n*-alkanes. This allows interpretation of the *n*-C_{17} hydrocracking selectivity data as a function of alkene coverage instead of zeolite catalyst topology.

2. Discussion

2.1. *n*-Alkane hydroconversion mechanism

In alkane hydroconversion, a metal site dehydrogenates alkanes into an alkene, an acid site converts the alkene into another isomer or a cracking product, whereupon the metal site hydrogenates the converted alkene back into an alkane [28–30]. When starting with an *n*-alkane, the hydroconversion can be described as a series of consecutive hydroisomerization steps, each increasing the degree of branching [30–32]. If one simplifies this process by only considering methyl group branches, the hydroisomerization of an *n*-alkane of N carbon atoms can be described as illustrated in Fig. 1.

In addition to the hydroisomerization reactions that change the degree of branching, there are also those that change the distribution of branching toward thermodynamic equilibrium [33–36]. None of the hydroisomerization reactions equilibrate completely because they compete with consecutive hydrocracking reactions that decompose the isomers [31,33–38]. The probability of a molecule undergoing a hydrocracking reaction increases with increasing degree of branching, because more extensively branched isomers afford the formation of more stable carbocationic hydrocracking transition states (Fig. 2) [32–36]. For *n*-alkanes as short as *n*-C_{10} the sequential series of hydroisomerization reactions is interrupted at the trimethylheptane stage, since very few trimethylheptanes desorb intact [33,39]. The first reason for the extremely low trimethylheptane yield is that trimethylheptanes have a significantly higher gas-phase Gibbs free energy of formation than the less branched isomers (Table 1) [27], so that they form only in relatively low concentrations to begin with. A second reason for the extremely low trimethylheptane yield is that $\alpha\alpha\gamma$-trimethlheptanes hydrocrack significantly more rapidly than any dimethylalkane [32–36]. Furthermore, trimethylheptanes that are not an $\alpha\alpha\gamma$-trimethylheptane are only

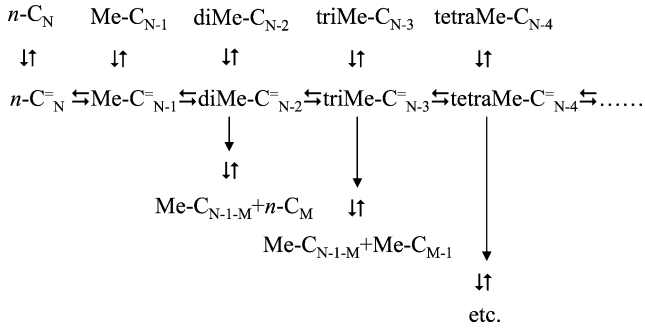

Fig. 1. *n*-Alkane hydroconversion mechanism [28–30]: *n*-alkane feed and hydroisomerization products (top) dehydrogenate into alkene intermediates (vertical ⇆, e.g., Pt catalyzed). Alkenes hydroisomerize in a chain of acid-catalyzed hydroisomerization reactions (horizontal ⇆). With increasing degree of branching it is increasingly more likely that isomers crack (vertical →, acid catalyzed) and hydrogenate into a smaller alkanes (vertical ⇆, e.g., Pt catalyzed).

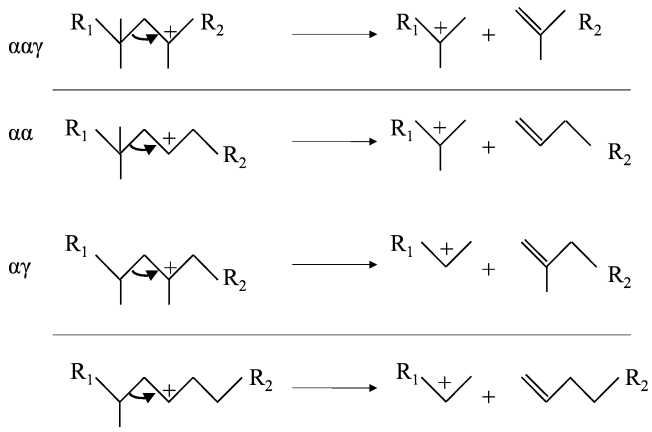

Fig. 2. Hydrocracking mechanism of the isomers that hydrocrack most easily [32–36] $\alpha\alpha\gamma$-trimethylalkane hydrocracking (top, R_1, R_2 a $H(CH_2)_x$-moiety with $x \geqslant 0$) involves only the most stable, tertiary carbocation transition states and—therefore—has the highest rate. $\alpha\gamma$- and $\alpha\alpha$-dimethylalkane hydrocracking involves both a tertiary and a less stable secondary carbocation transition state and—therefore—has a lower rate. Monomethylalkane hydrocracking involves secondary carbocations only, and—therefore—has a much lower rate than reactions involving at least one tertiary carbocation [32–36].

Table 1
Gas-phase Gibbs free energies of formation, ΔG_f (kJ/mol), of the various isomers relevant for hydrocracking at 500 K [27]

	ΔG_f		ΔG_f		ΔG_f
n-C_{10}	233	2,2-DMC_8	232	2,2,4-TMC_7	239
2-MC_9	231	2,4-DMC_8	236	2,4,4-TMC_7	240
3-MC_9	231	3,3-DMC_8	233	3,3,5-TMC_7	240
4-MC_9	231	3,5-DMC_8	232		
5-MC_9	234	4,4-DMC_8	233		

x, y-DMC_8 and x, y, z-TMC_7 are dimethyloctane and trimethyloctane isomers with methyl groups at positions x, y, and z, respectively.

a few rapid methyl shifts away from forming an $\alpha\alpha\gamma$-trimethylheptane, which in turn readily undergo hydrocracking reactions.

The thermodynamic and kinetic reasons for a low intact trimethylheptane yield notwithstanding, trimethylheptenes do in fact form and can be traced in the hydrocracking product slates as a high proportion of branched products (formed through $\alpha\alpha\gamma$-trimethylalkene hydrocracking) as compared to linear products (formed through $\alpha\alpha$- and $\alpha\gamma$-dimethylalkene hydrocracking (Fig. 2)). The extent of trimethylheptene formation and hydrocracking depends on the concentration of their dimethyloctene precursors (Fig. 1). Dimethylalkenes and -alkanes can build up more if a larger number of alkenes compete for adsorption at the acid sites [30–32]. Increased competitive adsorption reduces the average residence time of an alkene at an acid site and—thereby—increases its chances of desorbing as is rather than as a cracking product [30–32]. Thus, a decrease in the average alkene residence time at the acid sites enables the isomers to progress further through the sequence of consecutive reactions and approach thermodynamic equilibrium more closely as they do so [29–32,40]. Naturally, competitive adsorption between alkenes is maximal and the average alkene residence time at the acid sites is minimal when the acid sites are maximally covered with alkenes.

Early discussions of hydroprocessing catalysis examined the relationship between acid site coverage by alkenes and (a) the comparative activity levels of the acid function and the (de)hydrogenation function and (b) the mass transport rate between the two functions [29–32]. However, in later discussions the focus gravitated toward an assessment of how the catalyst compares to the theoretical concept of an "ideal" [31,32] or "well-balanced" [22,39,40] case. Catalysts are considered ideal or well-balanced bifunctional catalysts if (1) the activity of the (de)hydrogenation and acidic function are "balanced," i.e., they process all molecules in tandem, so that there is no monofunctional catalysis, and (2) alkene transport between (de)hydrogenation and acidic function is very fast as compared to the reaction rates so that the maximum (thermodynamic equilibrium) alkene concentration is maintained evenly dispersed throughout the catalyst at all times [32]. In principle this implies that catalysts are closest to ideal or are better balanced when the acid sites are more highly covered with alkenes. However, it is not clear how one should accommodate low yields of methane and ethane that indicate some monofunctional, Pt-catalyzed cracking (as in Refs. [22,41]). We prefer discriminating between the catalysts based on the alkene coverage of the acid sites, because this is a more fundamental notion that relates directly to the extent to which n-alkanes progress through the sequence of consecutive reactions before hydrocracking and—therefore—to the branched hydrocracking product yield (Fig. 1).

We will now evaluate how this mechanism can explain the experimental hydrocracking product slates at high, intermediate, and low alkene coverage. Each of the three cases starts out with deducing the relative alkene coverage from an analysis of the n-C_{10} hydrocracking product slate. Subsequently other properties of the product slate as an apparent function of alkene coverage are discussed.

2.2. Product slate analysis: high alkene coverage

2.2.1. Assessment alkene coverage

Fig. 3A illustrates a hydrocracking product slate that was obtained on very small crystals of MOR-type zeolite with a low acid site density [41]. The product distribution contains ~ 200 mol hydrocracking products per 100 mol C_{10} hydrocracked, and only 13% of the 100% i-C_7 that formed initially (Fig. 4) [10] has hydroisomerized into n-C_7 [41], indicating that the product slate was obtained in a regime in which very few of the initial hydrocracking products go on to partake in consecutive reactions. When the posthydrocracking consecutive reactions are minimal, the ratio of mol n-alkane hydrocracking products per 100 mol alkane feed hydrocracked quantifies the percentage of $\alpha\alpha$- and $\alpha\gamma$-dimethylalkane hydrocracking [33]. Measured by this yardstick, the product slate consists of

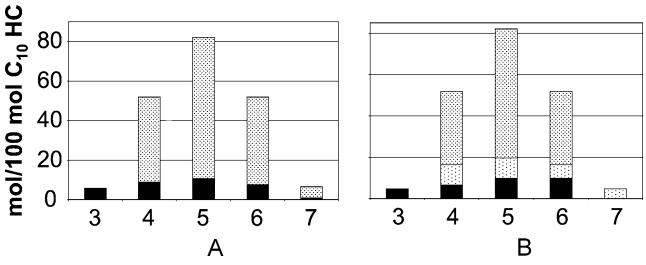

Fig. 3. Yield of decane hydrocracking products (mol/100 mol C_{10} hydrocracked) as a function of carbon number. (A) Experimental product slate reported for very small, low acid site density MOR-type zeolite crystals (*n*-alkanes are in black, isoalkanes in gray) [41], (B) calculated product slate in which we fitted the experimental *n*-alkanes with those generated by hydrocracking a dimethylalkane fraction at thermodynamic equilibrium (*n*-alkanes are in black (bottom), isoalkanes in light gray (middle)), and in which we attributed the remainder (isoalkanes in dark gray (top)) to trimethylalkane hydrocracking. The small quantities of ethane and nonane produced by Pt-catalyzed hydrogenolytic cracking [41]) were not included.

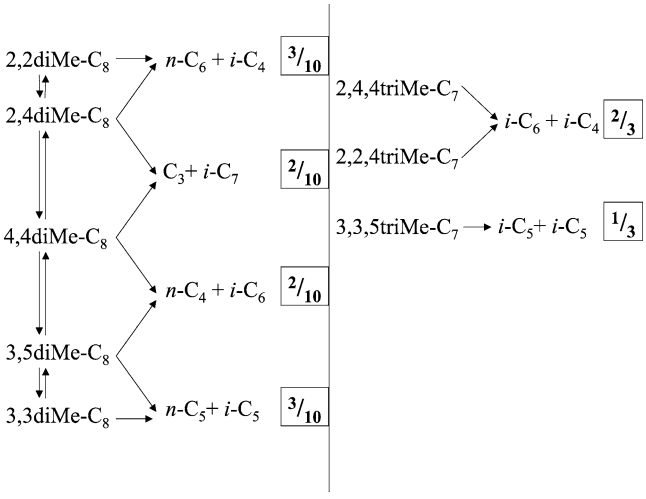

Fig. 4. The hydrocracking precursors and products obtained applying the mechanism shown in Fig. 2 to C_{10}. In the boxes are the chances for forming hydrocracking products assuming that all $\alpha\gamma$- and $\alpha\alpha$-dimethyloctanes are available in equal amounts and that there is no preference for hydrocracking. The same was done for $\alpha\alpha\gamma$-trimethylheptane hydrocracking. Only hydrocracking routes involving at least one tertiary carbocation transition state are included because only these routes are fast enough to make an impact [32–36]. When there are only secondary carbocation transition states involved (as in monomethylalkane hydrocracking) hydrocracking occurs at a significantly lower rate [32–36].

$\sim$ 35% $\alpha\alpha$- and $\alpha\gamma$-dimethyloctane hydrocracking products and $\sim$ 65% $\alpha\alpha\gamma$-trimethylheptane hydrocracking products (Table 2). Since propane, C_3, and heptane, C_{N-3}, can only form through $\alpha\alpha$- and $\alpha\gamma$-dimethyloctane hydrocracking and not through $\alpha\alpha\gamma$-trimethylheptane hydrocracking, the sum of the propane and heptane yield provides another, independent yardstick for the relative contribution of $\alpha\alpha$- and $\alpha\gamma$-dimethyloctane hydrocracking (Table 3). When compared to the other catalysts in this study, this catalyst exhibits the lowest combined propane and heptane yield (Table 3). Thus, with this catalyst system, *n*-C_{10} moved furthest along the chain of consecutive hydroisomerization reactions and formed the highest amount of branched hydrocracking products and the lowest amount of C_3 and C_{N-3} hydrocracking products of all the catalysts studied (Tables 2 and 3). Correspondingly this hydrocracking product slate was obtained under conditions with the highest acid site alkene coverage of the catalysts under study.

Table 2
Fraction of *n*-alkanes in the hydrocracking products (mol per 100 mol feed alkane hydrocracked) obtained from MOR- [41], FAU- [31], and intergrown EMT- and FAU-type zeolites [22] reported at $\sim$ 35, $\sim$ 50, $\sim$ 48% hydrocracking, respectively

Feed C No.	MOR (mol *n*-alkane/ 100 mol feed hydrocracked)	FAU (mol *n*-alkane/ 100 mol feed hydrocracked)	FAU/EMT (mol *n*-alkane/ 100 mol feed hydrocracked)
9		70	76
10	35	62	70
11		54	65
12		48	57
13			57
14			42
15			42
16			42
17			49

For C_{10} the yield of *n*-alkane per 100 mol feed alkane hydrocracked reflects the percentage $\alpha\alpha$- or $\alpha\gamma$-dimethylalkane hydrocracking (see Figs. 2 and 4). For longer *n*-alkanes it becomes an increasingly inaccurate measure for the contribution from dimethylalkane hydrocracking due to an increased likelihood of posthydrocracking hydroisomerization reactions of the initially formed *n*-alkane hydrocracking products.

Table 3
Combined propane, C_3, and complementary alkane hydrocracking product, C_{N-3}, yield (with *N* the feed carbon number) per 100 mol feed alkane hydrocracked, obtained from MOR- [41], FAU- [31], and intergrown FAU- and EMT-type zeolites [22] reported at $\sim$ 35, $\sim$ 50, and $\sim$ 48% hydrocracking, respectively. Since C_3 and C_{N-3} are formed through $\alpha\alpha$- or $\alpha\gamma$-dimethylalkane hydrocracking but not through $\alpha\alpha\gamma$-trimethylalkane hydrocracking (Fig. 4) they are a yardstick for the relative contributions of these hydrocracking pathways to the hydrocracking product slate

Feed C No.	MOR $C_3 + C_{N-3}$ (mol/100 mol feed hydrocracked)	FAU $C_3 + C_{N-3}$ (mol/100 mol feed hydrocracked)	FAU/EMT $C_3 + C_{N-3}$ (mol/100 mol feed hydrocracked)
9		40	45
10	12	27	36
11		20	25
12		12	19
13		14	18
14		10	8
15			9
16		10	8
17			8

2.2.2. Product slate analysis

In addition to establishing the extent to which an *n*-alkane can progress through the sequence of consecutive hydroisomerization reactions, the hydrocracking product slate at this high coverage of the acid sites with alkenes provides a base case for the most complete thermodynamic equilibration within the dimethyl- and trimethylalkane fractions. The extent of thermodynamic equilibration between the dimethy-

lalkanes during hydrocracking can be assessed by comparing the *n*-alkane distribution in the experimental hydrocracking product slate with the distribution calculated from a mixture of $\alpha\alpha$- and $\alpha\gamma$-dimethylalkane at thermodynamic equilibrium. In the catalytically relevant temperature regime (near 500 K) such an equilibrated mixture contains approximately 26, 10, 21, 22, and 21 mol% of 2,2-, 2,4-, 3,3-, 3,5-, and 4,4-dimethyloctane, respectively [27]. The dimethyloctane hydrocracking product slate calculated from this mixture (assuming that there is no preferential cracking) (Fig. 4) contains 8, 11, 16, and 15 mol per 100 mol C_{10} hydrocracked of C_3, *n*-C_4, *n*-C_5, and *n*-C_6, respectively. The relative amounts of these *n*-alkanes match remarkably well with those of the experimental product slate (Fig. 3). Apparently, the rate of hydrocracking and hydroisomerization of $\alpha\alpha$- and $\alpha\gamma$-dimethylalkane in the experimental catalyst is sufficiently slow as compared to the rate of the equilibrating methyl shift reactions that the mixture is virtually able to maintain thermodynamic equilibrium among the hydrocracking dimethylalkanes.

Similarly, the composition of a thermodynamically equilibrated mixture of $\alpha\alpha\gamma$-trimethylheptanes (at 500 K) was calculated. It consists of approximately 38, 32, and 30% 2,2,4-, 2,4,4- and 3,3,5-trimethylheptane, respectively [27]. If all three of the thermodynamically equilibrated isomers hydrocrack at the same rate, they yield 70, 60, and 70 mol per 100 mol C_{10} hydrocracked of *i*-C_4, *i*-C_5, and *i*-C_6, respectively (Fig. 4). By contrast, the experimental product slate shows a significantly higher *i*-C_5 yield than either the *i*-C_4 or *i*-C_6 yield (Fig. 3)—also when the yield is adjusted for the likely contribution from $\alpha\alpha$- and $\alpha\gamma$-dimethylalkane (Fig. 3B). Since 3,3,5-trimethylheptane yields *i*-C_5 whereas both 2,2,4- and 2,4,4-trimethylheptane yield *i*-C_4 + *i*-C_6 (Fig. 4), the excessive *i*-C_5 yield indicates that the trimethylheptane hydrocracking precursors contain more 3,3,5-trimethylheptane and less 2,2,4- and 2,4,4-trimethylheptane than at thermodynamic equilibrium. Apparently the most rapid hydrocracking process (i.e., that of $\alpha\alpha\gamma$-trimethylalkanes [32]) is too fast to allow methyl shifts to fully establish thermodynamic equilibrium between the trimethylheptanes.

In the absence of thermodynamic equilibrium (and shape selectivity) hydroisomerization kinetics dictates the composition of the hydrocracking product slate. To evaluate this kinetic effect it is useful to consider the probability of formation of the individual trimethylheptanes from an equimolar (i.e., thermodynamically equilibrated) mixture of all their dibranched precursors (Fig. 5). This analysis shows that the

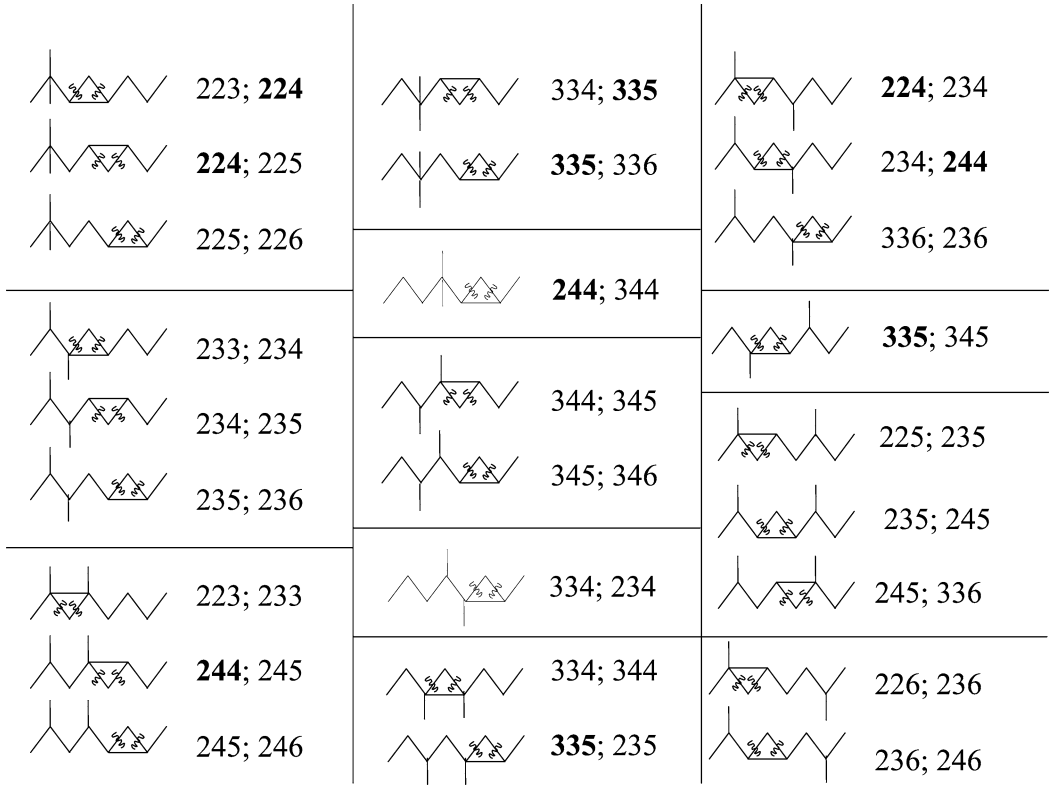

Fig. 5. Assessment of the kinetic preference for forming methyl groups near the center of the chain. Δ and ∇ represent the protonated dialkylcyclopropyl groups that are the transition states in alkane hydroisomerization. If all of the 12 different dimethyloctanes are present in equimolar quantities, and if there is no preference for forming and opening any particular transition state (the triangular part of the structures), the chances for forming 2,2,4-, 2,4,4,- and 3,3,5-trimethylheptane are $(1/6+1/6+1/6)/12 = 6/144$, $(1/6+1/2+1/6)/12 = 10/144$, and $(1/4+1/4+1/4+1/2)/12 = 15/144$, respectively. Methyl shifts between the different trimethylheptanes will shift the distribution toward thermodynamic equilibrium (approximately an equimolar distribution of all 16 trimethylheptanes) and will—thereby—reduce this outspoken statistic preference for forming methyl groups depending on their proximity to the center of the alkane chain.

probability of formation of $\alpha\alpha\gamma$-branched isomers is dependent on the proximity of the methyl groups to the center of the alkane; for reasons of symmetry there are fewer permutations of the precursor transition state closer to the center. Preferential formation of $\alpha\alpha\gamma$-methyl groups at or near the center of an alkane results in preferential hydrocracking at or near the center of the alkane. In contrast $\alpha\alpha$- and $\alpha\gamma$-dimethylalkane hydrocracking is slow enough to allow the dimethylalkanes to approach thermodynamic equilibrium more closely (by rapid methyl shifts) before hydrocracking sets in, so that these isomers do not exhibit a kinetic preference for center hydrocracking comparable to that of trimethylalkane hydrocracking (Fig. 3).

Having established how far an n-C_{10} can progress through the sequence of consecutive hydroisomerization reactions and how closely the isomers within the dialkyl- and trialkylalkanes can approach thermodynamic equilibrium at high alkene coverage, we can now evaluate the effect on the progress through the reaction chain and the approach to equilibrium at intermediate and low alkene coverage and with n-alkane feeds longer than n-C_{10}.

2.3. Product slate analysis: intermediate alkene coverage

2.3.1. Assessment alkene coverage

Fig. 6 illustrates hydrocracking product slates that were obtained on a low acid site density FAU-type zeolite [31,32]. The product distribution contains $\sim$ 200 mol hydrocracking products per 100 mol C_{10} hydrocracked, and only 9% of the 100% i-C_7 formed initially (Fig. 4) [10] has hydroisomerized into n-C_7 [31,32] indicating that these product slates were obtained in a regime in which very few of the initial hydrocracking products go on to partake in consecutive reactions. With consecutive reactions kept to a minimum, the n-alkane hydrocracking product yield is a measure for the extent of $\alpha\alpha$- and $\alpha\gamma$-dimethylalkane hydrocracking. Measured by this yardstick, the product slate consists of $\sim$ 62% $\alpha\alpha$- and $\alpha\gamma$-dimethyloctane hydrocracking products and only $\sim$ 38% $\alpha\alpha\gamma$-trimethylheptane hydrocracking products. This is a significant increase from the $\sim$ 35% $\alpha\alpha$- and $\alpha\gamma$-dimethyloctane and $\sim$ 65% $\alpha\alpha\gamma$-trimethylheptane hydrocracking products seen in the product slate obtained with a high alkene coverage (Fig. 3). Similarly the increase in C_3 and C_{N-3} yield (Table 3) indicates an increase in $\alpha\alpha$- and $\alpha\gamma$-dimethyloctane hydrocracking at the expense of $\alpha\alpha\gamma$-trimethylheptane hydrocracking when going from conditions of high alkene coverage to the current conditions. Thus, under these conditions n-C_{10} progressed less far along the chain of consecutive hydroisomerization reactions and formed a smaller amount of branched and a higher amount of C_3 plus C_{N-3} hydrocracking products than observed under the conditions with high acid site alkene coverage (Tables 2 and 3). Correspondingly this hydrocracking product slate was obtained under conditions with some lower "intermediate" acid site alkene coverage.

This intermediate coverage product slate contains more n-C_4 and less n-C_6 than the high coverage product slate suggesting an increase in 4,4- and 3,5-dimethyloctane hydrocracking at the expensive of 2,2- and 2,4-dimethyloctane hydrocracking (Fig. 4). This constitutes a shift away from thermodynamic equilibrium between the dimethyloctanes toward preferential formation and hydrocracking of isomers with methyl groups near the center of the alkane. Even though there is less $\alpha\alpha\gamma$-trimethylheptane hydro-

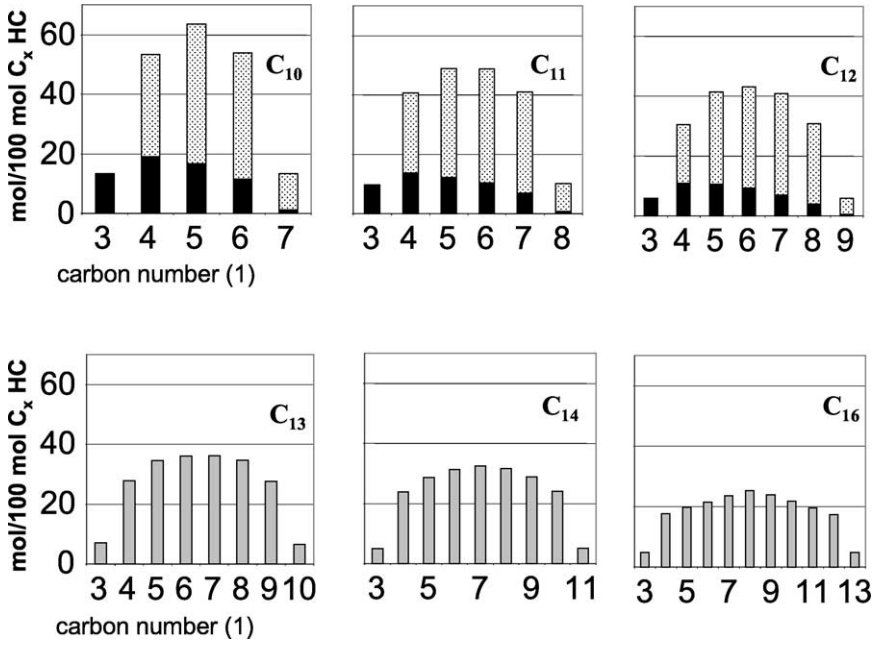

Fig. 6. Experimental hydrocracking product slates reported for low acid site density FAU-type zeolite with feeds ranging from n-C_{10} to n-C_{16} (n-C_{15} omitted) with n-alkanes in black, isoalkanes in light gray, and n- and isoalkanes combined in dark gray [31]. Irrespective of the feed length the histogram shows a single sharp maximum at the middle carbon atom(s).

cracking, the i-C_5 yield is still greater than the i-C_4 and i-C_6 yield (Fig. 4) suggesting that the chances of formation and hydrocracking $\alpha\alpha\gamma$-trimethylalkanes remain proportional of the proximity of the methyl groups to the center of the alkane chain. Thus, conditions with this intermediate alkene coverage are characterized by a shift in the hydrocracking pathway from $\alpha\alpha\gamma$-trimethylalkanes to $\alpha\alpha$- and $\alpha\gamma$-dimethylalkanes and by a kinetic preference for forming and hydrocracking both dimethyl- and trimethylalkanes depending on the proximity of the methyl groups to the center of the alkane chain.

When feed alkane chain length increases beyond C_{10} the fraction of n-alkanes in the hydrocracking product slate decreases (Table 2). Since the alkene-to-alkane ratio at thermodynamic equilibrium increases with increasing alkane chain length [27], the coverage of the acid sites by alkenes also increases with increasing feed alkane chain length. This shifts the hydrocracking pathway from $\alpha\alpha$- and $\alpha\gamma$-dimethylalkanes to $\alpha\alpha\gamma$-trimethylalkanes and results in fewer n-alkane hydrocracking products.

2.3.2. Product slate analysis for n-alkanes longer than n-C_{10}

Analyzing the thermodynamic and kinetic factors that influence the hydrocracking product slate of the n-alkane feed molecules longer than n-C_{10} is not as straightforward as with n-C_{10}, because the relevant thermodynamic data are not readily available. However, they can be obtained by extrapolation from those available on C_{10}: all three C_{10} $\alpha\alpha\gamma$-trimethylalkanes have a nearly identical Gibbs free energy of formation in the gas phase (Table 1) [27], so that an equimolar mixture of all $\alpha\alpha\gamma$-trimethylalkane isomers approaches the thermodynamic equilibrium distribution reasonably well. If we approximate the thermodynamic equilibrium distribution of $\alpha\alpha\gamma$-trimethylalkane isomers for molecules longer than C_{10} with an equimolar mixture of all $\alpha\alpha\gamma$-trimethylalkanes, the resultant hydrocracking product slate of an n-alkane with N carbon atoms is an even distribution of isoalkanes from carbon number 4 to $N-4$. As with C_{10}, this calculated flat profile is not observed experimentally (Fig. 6), because $\alpha\alpha\gamma$-trimethylalkanes have more precursors, and therefore a higher chance of formation, with increasing proximity of the $\alpha\alpha\gamma$ methyl groups to the center of the chain. Accordingly, all experimental product slates are skewed toward hydrocracking at the center of the alkane irrespective of the length of the alkane feed (Fig. 6).

For C_{10} we were able to infer from the n-alkane hydrocracking product distribution that $\alpha\alpha$- and $\alpha\gamma$-dimethylalkanes hydrocracking exhibits a kinetic bias toward hydrocracking alkanes with the methyl groups closer to the center of the alkane similar to that of $\alpha\alpha\gamma$-trimethylalkane hydrocracking. For alkanes longer than C_{10} the increased likelihood of posthydrocracking consecutive hydroisomerization reactions of the relatively long n-alkane hydrocracking products [42–44] impedes the inference of a similar kinetic bias.

Thus, n-alkanes progresses less far through the sequence of consecutive hydroisomerization reactions and dialkyl- and trialkylalkanes and do not approach thermodynamic equilibrium as closely when the alkene coverage of the acid sites drops from high to intermediate levels. At intermediate alkene coverage hydrocracking of $\alpha\alpha\gamma$-trimethylalkenes with methyl groups closest to the center of the alkane chain continues to dominate the hydrocracking product slates. The hydrocracking product slates are not markedly influenced by the FAU-type aluminosilicate topology of the catalyst (shape selectivity), for similar (though less detailed) product slates were reported for amorphous aluminosilicate catalysts [29,30]. We can now evaluate to what extent these conclusions extrapolate to conditions of low acid site alkene coverage.

2.4. Product slate analysis: low alkene coverage

2.4.1. Assessment alkene coverage

Fig. 7 illustrates hydrocracking product slates that were obtained on an intergrowth of EMT- and FAU-type zeolites [22–24,45,46] and on a BEA-type zeolite [47]. The C_{10} hydrocracking product distribution contains ~ 200 mol hydrocracking products per 100 mol C_{10} hydrocracked, and 21% of the 100% i-C_7 formed initially (Fig. 4) [10] has hydroisomerized into n-C_7 [22]. This higher C_7 hydroisomerization (and lower symmetry of the product slate) indicates that the product slate was obtained in a regime in which more of the initial hydrocracking products go on to partake in consecutive reactions than in any of the C_{10} product slates discussed above. A larger extent of posthydrocracking consecutive reactions introduces a larger error in the quantification of the percentage of $\alpha\alpha$- and $\alpha\gamma$-dimethylalkane hydrocracking utilizing the ratio of mol n-alkane hydrocracking per 100 mol alkane feed hydrocracked. Nevertheless, the product slate contains as many as $\sim 70\%$ $\alpha\alpha$- and $\alpha\gamma$-dimethyloctane and as few as $\sim 30\%$ $\alpha\alpha\gamma$-trimethylheptane hydrocracking products [22] (Table 2). Since propane, C_3, and heptane, C_{N-3}, can only form through $\alpha\alpha$- and $\alpha\gamma$-dimethyloctane hydrocracking and not through $\alpha\alpha\gamma$-trimethylheptane hydrocracking, the combined yield of the propane and heptane provides another, independent yardstick for the relative contribution of $\alpha\alpha$- and $\alpha\gamma$-dimethyloctane hydrocracking (Table 3). When compared to the other catalysts in this study, this catalyst exhibits the highest combined propane and heptane yield (Table 3). It is consistent with the conclusion that n-C_{10} progressed least far along the chain of consecutive hydroisomerization reactions and formed the lowest amount of branched hydrocracking products and the highest amount combined C_3 and C_{N-3} of all the catalysts studied (Tables 2 and 3). Correspondingly these hydrocracking product slates were obtained under conditions with the lowest alkene coverage of the catalysts under study.

The comparatively high n-C_4 and low n-C_6 yield in the C_{10} hydrocracking product slate obtained under conditions

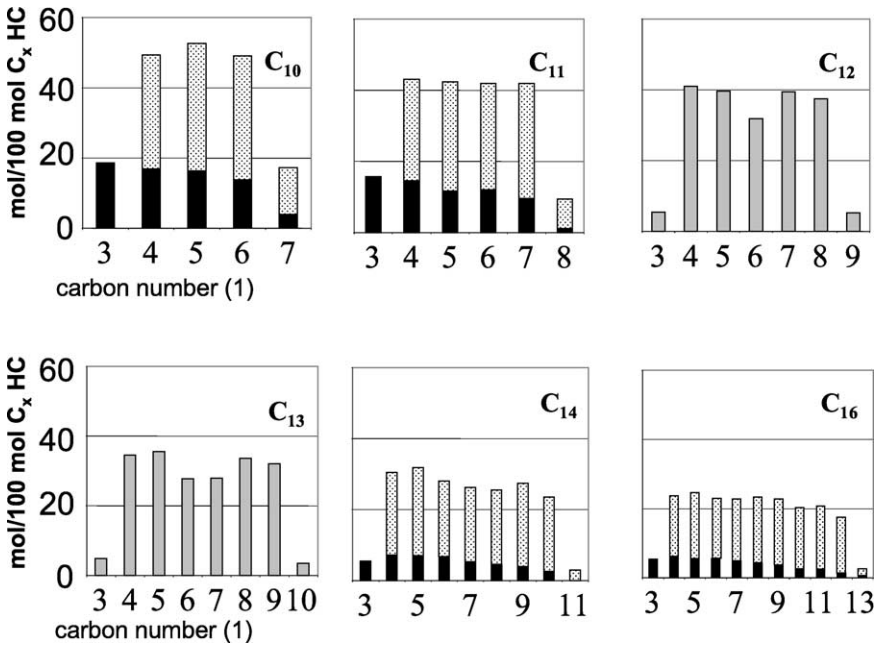

Fig. 7. Experimental hydrocracking product slates reported for high acid site density relatively large crystals of EMT- and FAU-type zeolites (n-C_{10}, n-C_{11}, n-C_{14}, n-C_{16} [22]) and for BEA-type zeolites (n-C_{12} and n-C_{13} [47]). These three structures yield virtually identical product slates for n-C_{12} and n-C_{13} (cf. Refs. [22,47]). n-Alkanes are shown in black, isoalkanes in light gray, and all-gray bars represent cases in which the normal/iso distribution was not published. For an n-C_{11} the histogram exhibits a broad maximum from C_4 to C_7, for n-C_{12} it exhibits two maxima at $C_{4–5}$ and $C_{7–8}$, for n-C_{13} two maxima at $C_{4–5}$ and $C_{8–9}$, for n-C_{14} two maxima at $C_{4–5}$ and $C_{9–10}$, for C_{16} the features are blurred due to consecutive hydrocracking. Small quantities of methane, ethane, and C_{N-1} and C_{N-2} produced by Pt-catalyzed hydrogenolytic cracking were not included.

of low alkene coverage indicates a preference for hydrocracking $\alpha\alpha$- and $\alpha\gamma$-dimethyloctane with methyl groups closest to the center of alkane that is comparable to that observed at intermediate alkene coverage (cf. Figs. 6 and 7).

As with the intermediate coverage product slate, the n-alkane hydrocracking product yield decreases with increasing chain length, suggesting a shift in the hydrocracking pathway from $\alpha\alpha$- and $\alpha\gamma$-dimethylalkane hydrocracking toward $\alpha\alpha\gamma$-trimethylheptane hydrocracking (Table 2). Such a shift would be in agreement with the increased alkene-to-alkane ratio expected for longer feed molecules at thermodynamic equilibrium.

2.4.2. Product slate analysis for n-alkanes longer than n-C_{10}

Interestingly, at this low alkene coverage feed molecules longer than C_{10} no longer produce hydrocracking product slates consisting of histograms with a single sharp maximum (Fig. 7). Instead of a single sharp maximum in the middle of the histogram irrespective of the feed alkane length (Fig. 6), there is either a very broad maximum (Fig. 7, C_{11}) or there are several maxima (Fig. 7, $C_{12–17}$) depending on the feed alkane length (Fig. 7) [22]. Product slates virtually identical to those reported for these EMT/FAU intergrowths were reported for high acid site density FAU-type zeolites [22,23] and for BEA-type zeolites [47].

To disentangle shape selectivity from thermodynamic and kinetic effects, we approximate the thermodynamic equilibrium of $\alpha\alpha$- and $\alpha\gamma$-dimethylalkane of alkanes longer than C_{10} with an equimolar mixture, as we did with our analysis of the $\alpha\alpha\gamma$-trimethylalkane hydrocracking products. Fig. 8 illustrates the product slates calculated by assuming no preferential hydrocracking of any particular isomer. Interestingly, the calculated product slates (Fig. 8) reproduce the most salient features of the experimental ones remarkably well (Fig. 7). This suggests that the reason for the kaleidoscopic change in the features of the experimental and the calculated product slates as a function of alkane chain length is the low symmetry of $\alpha\alpha$- and $\alpha\gamma$-dimethylalkane hydrocracking as compared to $\alpha\alpha\gamma$-trimethylalkane hydrocracking (Fig. 2).

Naturally there are discrepancies between the experimental and the calculated hydrocracking product slates, for the calculated slates do not account for (i) $\alpha\alpha\gamma$-trimethylalkane hydrocracking, (ii) the kinetic bias for forming and cracking alkanes with methyl groups near the center of the chain, (iii) the difference in rate between $\alpha\alpha$- and $\alpha\gamma$-dimethylalkane hydrocracking [35–38], (iv) likely [43,44] posthydrocracking consecutive isomerization reactions, and (v) slight differences in Gibbs free energies of formation of the individual isomers. The crudeness of our assumptions notwithstanding, the remarkable similarities between calculated and experimental histograms strongly suggest that the multiple maxima in the experimentally observed selectivity pattern are predominantly the result of a change in the hydrocracking pathway from the highly symmetric hydrocracking of $\alpha\alpha\gamma$-trimethylheptane to the significantly less symmetric

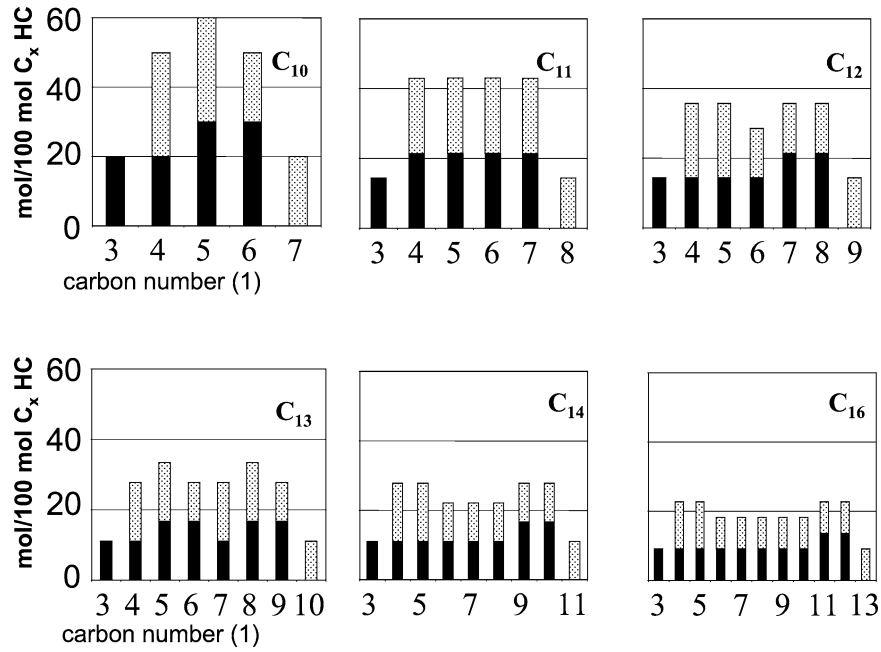

Fig. 8. Calculated hydrocracking product slates obtained from an equimolar mixture of $\alpha\gamma$- and $\alpha\alpha$-dimethyloctanes assuming no preferential hydrocracking (i.e., expanding the method illustrated in Fig. 4 to longer alkane lengths). *n*-Alkanes are shown in black, isoalkanes in light gray. As with the experimental product slates (Fig. 7), the histogram for an *n*-C_{11} feed exhibits a broad maximum from C_4 to C_7, that for *n*-C_{12} two maxima at $C_{4–5}$ and $C_{7–8}$, that for *n*-C_{13} two maxima at $C_{4–5}$ and $C_{8–9}$, that for *n*-C_{14} two maxima at $C_{4–5}$ and $C_{9–10}$, and that for C_{16} two maxima at $C_{4–5}$ and $C_{10–11}$.

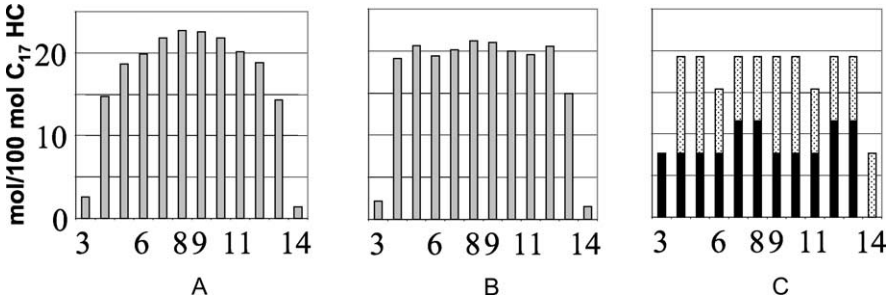

Fig. 9. Change of the C_{17} hydrocracking product slates with increasing coverage of the acid sites by alkenes (from B to A due to steaming followed by acid leaching) as reported for intergrowths of EMT- and FAU-type zeolites [23], and a comparison between an experimental C_{17} hydrocracking product slate dominated by $\alpha\gamma$- and $\alpha\alpha$-dimethylpentadecane hydrocracking (B) and a calculated slate generated assuming (1) a precursor mixture consisting of an equimolar mixture of all $\alpha\gamma$- and $\alpha\alpha$-dimethylpentadecanes and (2) no preferential hydrocracking of any particular isomer (C).

hydrocracking of $\alpha\alpha$- and $\alpha\gamma$-dimethyloctane as a result of a low degree of alkene coverage.

The sensitivity of the hydrocracking product slate to the alkene coverage of the acid sites has been documented particularly well for *n*-C_{17} hydroconversion [23]. Severe steaming followed by acid leaching an intergrowth of FAU- and EMT-type zeolites transformed a hydrocracking product slate with two minima (at C_6 and C_{11}, Fig. 9B) into a product slate with a single maximum in the middle (Fig. 9A). The former product slate is typical for $\alpha\alpha$- and $\alpha\gamma$-dimethylalkane-dominated hydrocracking, the latter for $\alpha\alpha\gamma$-trimethylalkane-dominated hydrocracking (cf. Figs. 9B and C). Since $\alpha\alpha\gamma$-trimethylalkane-dominated hydrocracking is typical for a high alkene coverage and $\alpha\alpha$- and $\alpha\gamma$-dimethylalkane for a low alkene coverage, the increased importance of $\alpha\alpha\gamma$-trimethylalkane hydrocracking following severe steaming and acid leaching indicates an increase in the alkene coverage. Severe steaming and acid leaching dramatically decrease the acid site density, increase the accessibility of these acid sites through the formation of mesoporous mass transport shortcuts [21], but do not decrease the alkene concentration. The net result is a higher, more homogeneous alkene concentration concurrent with a lower acid site density. With more alkenes competing for adsorption at fewer acid sites the average alkene residence time at an acid site decreases, and alkenes will undergo fewer cycles per molecule and will have a commensurately higher chance of desorbing intact instead of being cracked before hydrogenating back into an alkane. This results in a buildup of more dibranched alkanes that in turn can build up more tribranched alkanes before hydrocracking. Thus, the change in hydrocracking product slate following

steaming and acid leaching illustrates how these processes increase the coverage of the acid sites with alkenes and—thereby—shift the hydrocracking pathway from $\alpha\alpha$- and $\alpha\gamma$-dimethylpentadecane toward $\alpha\alpha\gamma$-trimethyltetradecane hydrocracking.

Previously, the multimodal hydrocracking product distributions obtained on zeolites as diverse as FAU-, EMT- and BEA-type zeolites [26] were not attributed to variations in the dominant kinetic pathway with the alkene coverage of the acid sites. Instead they were attributed to features of the topologies of the specific zeolites employed [23,24,45,47], i.e., to some form of mass transfer or transition-state shape selectivity. We would expect to see noticeable different shape selectivity from the distinctly different FAU, EMT, BEA, and MOR topologies [26]. The marked similarities of the product slates obtained on FAU- and MOR-type zeolites on the one hand and on FAU-, EMT-, and BEA-type zeolites on the other suggest the presence of a generic mechanism independent of topology. Naturally, this does not imply that the differences among FAU-, EMT-, MOR-, and BEA-type zeolite topologies do not contribute to the selectivity in alkane hydroconversion. The diameter of the smallest constriction in these topologies decreases in the order of FAU > EMT > MOR > BEA [26]. Correspondingly, the alkene mobility will decrease in the same order, as will the coverage of the acid sites with alkenes at equal acid site density and equal zeolite crystal agglomerate size. However, this paper illustrates that catalyst topology is unlikely to be the prime cause of the discussed alterations to the kinetic network in n-alkane hydroconversion.

3. Conclusions

When acid sites are highly covered with alkenes, $\alpha\alpha\gamma$-trimethylalkenes constitute the majority of the hydrocracking precursors. These have a kinetic bias to hydroisomerize so that the methyl groups are at the center of the alkane, yielding a hydrocracking product distribution with a single sharp maximum at the middle carbon number(s) [29].

With decreasing alkene coverage of the acid sites, the alkanes progress less far through the sequence of consecutive hydroisomerization reactions and hydrocracking shifts away from $\alpha\alpha\gamma$-trimethylalkanes and toward $\alpha\alpha$- and $\alpha\gamma$-dimethylalkanes. When this shift is sufficiently large, it changes the appearance of the hydrocracking product distribution from a distribution with a single maximum in the middle of the distribution, irrespective of the alkane feed length, to distributions with multiple maxima and with an appearance that varies strongly with alkane feed length. The position of the maxima in these distributions and the strong dependence on feed length of the features of these distributions are related to the low symmetry of $\alpha\alpha$- and $\alpha\gamma$-dimethylalkane hydrocracking as compared to $\alpha\alpha\gamma$-trimethylalkane hydrocracking. Calculated hydrocracking product slates obtained by approximating the thermodynamic equilibrium distribution of $\alpha\alpha$- and $\alpha\gamma$-dimethylalkanes with an equimolar mixture reproduce both the maxima and their chain length dependence remarkably well.

The features now attributed to $\alpha\alpha$- and $\alpha\gamma$-dimethylalkanes hydrocracking were previously attributed to features somehow typical for FAU-, EMT-, and BEA-type zeolites. Based on the similarities of the product slates reported for these dissimilar zeolite structures we would argue against such an explanation, favoring an explanation that is not based on zeolite topology, namely a change in the reaction network as a result of a decrease in the alkene coverage of the acid sites.

Acknowledgments

These investigations are supported in part by the Netherlands Research Council for Chemical Sciences (CW) with financial aid from the Netherlands Technology Foundation, by the Netherlands Organization for Scientific Research (NWO) through PIONIER, by ChevronTexaco, and by the Stichting Nationale Computer Faciliteiten (National Computing Facilities Foundation) through the use of the supercomputer facilities. We thank the European Commission for a Marie Curie Individual Research Fellowship (to S.C.). We thank A. Kuperman, C. Wilson, C.H. Roemkens, D. Dubbeldam, and S.I. Zones, for their comments on our manuscript.

References

[1] P.M.M. Blauwhoff, J.W. Gosselink, E.P. Kieffer, S.T. Sie, W.H.J. Stork, in: J. Weitkamp, L. Puppe (Eds.), Catalysis and Zeolites, Springer, Berlin, 1999, pp. 437–538.
[2] R.H. Jensen, in: M. Guisnet, J.-P. Gilson (Eds.), Zeolites for Cleaner Technologies, Imperial College Press, 2002, pp. 75–103.
[3] M.M. Habib, A.J. Dahlberg, Hydrocarbon Eng. 7 (2002) 45–47.
[4] J.A.R. van Veen, in: M. Guisnet, J.-P. Gilson (Eds.), Zeolites for Cleaner Technologies, Imperial College Press, 2002, pp. 131–152.
[5] A. Corma, A. Martinez, in: M. Guisnet, J.-P. Gilson (Eds.), Zeolites for Cleaner Technologies, Imperial College Press, 2002, pp. 29–55.
[6] D.C. Kramer, B.K. Lok, R.R. Krug, ASTM Special Techn. Publ. STP 1407 (2001) 25–38.
[7] M. Daage, in: M. Guisnet, J.-P. Gilson (Eds.), Zeolites for Cleaner Technologies, Imperial College Press, 2002, pp. 167–187.
[8] J. Weitkamp, S. Ernst, L. Puppe, in: J. Weitkamp, L. Puppe (Eds.), Catalysis and Zeolites, Springer, Berlin, 1999, pp. 326–376.
[9] T.L.M. Maesen, M. Schenk, T.J.H. Vlugt, J.P. de Jonge, B. Smit, J. Catal. 188 (1999) 403–412.
[10] T.L.M. Maesen, M. Schenk, T.J.H. Vlugt, B. Smit, J. Catal. 203 (2001) 281–291.
[11] M. Schenk, B. Smit, T.J.H. Vlugt, T.L.M. Maesen, Angew. Chem. Int. Ed. 40 (2001) 736–739.
[12] M. Schenk, S. Calero, T.L.M. Maesen, L.L. van Benthem, M.G. Verbeek, B. Smit, Angew. Chem. Int. Ed. 41 (2002) 2499–2502.
[13] M. Schenk, S. Calero, T.L.M. Maesen, T.J.H. Vlugt, L.L. van Benthem, M.G. Verbeek, B. Smit, J. Catal. 214 (2003) 92–103.
[14] S.M. Csicsery, Zeolites 4 (1984) 202–213.
[15] S.M. Csicsery, Chem. Br. 21 (1985) 473–477.
[16] P.B. Weisz, Pure Appl. Chem. 52 (1980) 2091–2103.

[17] D. Dubbeldam, S. Calero, T.L.M. Maesen, B. Smit, Angew. Chem. Int. 42 (2003) 3630–3633.
[18] C.N. Satterfield, J.R. Katzer, W.R. Vieth, Ind. Eng. Chem., Fundam. 10 (1971) 478–486.
[19] J.C. Cheng, T.F. Degnan, J.S. Beck, Y.Y. Huang, M. Kalyanaraman, J.A. Kowalski, C.A. Loehr, D.N. Mazzone, Stud. Surf. Sci. Catal. 121 (1999) 53–60.
[20] G. Sastre, C.R.A. Catlow, A. Corma, J. Phys. Chem. B 103 (1999) 5187–5196.
[21] R. Szostak, Stud. Surf. Sci. Catal. 58 (1991) 153–199.
[22] J.A. Martens, M. Tielen, P.A. Jacobs, Stud. Surf. Sci. Catal. 46 (1989) 49–60.
[23] J.A. Martens, G.M. Vanbutsle, P.A. Jacobs, in: R. von Ballmoos, J.B. Higgins, M.M.J. Treacy (Eds.), Proceedings from the Ninth International Zeolite Conference, Vol. 2, Butterworth–Heinemann, Boston, 1993, pp. 342–355.
[24] J.A. Martens, P.A. Jacobs, in: E.G. Derouane, F. Lemos, C. Naccache, F. Ramão-Ribeiro (Eds.), Zeolite Microporous Solids: Synthesis, Structure, and Reactivity, in: NATO ASI Series, Vol. 352, Kluwer, Amsterdam, 1992, pp. 511–529.
[25] J.F. Denayer, G.V. Baron, J.A. Martens, P.A. Jacobs, J. Phys. Chem. B 102 (1998) 3077–3081.
[26] Ch. Baerlocher, W.M. Meier, D.H. Olson, Atlas of Zeolite Structure Types, 5th ed., Elsevier, Amsterdam, 2001; http://www.iza-structure.org/databases/, by Ch. Baerlocher, L.B. McCusker.
[27] D.R. Stull, E.F. Westrum Jr., G.C. Sinke, The Chemical Thermodynamics of Organic Compounds, Krieger, Malabar, FL, 1987.
[28] G.A. Mills, H. Heinemann, T.H. Milliken, A.G. Oblad, Ind. Eng. Chem. 45 (1953) 134–137.
[29] P.B. Weisz, Adv. Catal. 13 (1962) 137–190.
[30] H.L. Coonradt, W.E. Garwood, Ind. Eng. Chem. Proc. Des. Dev. 3 (1964) 38–45.
[31] J. Weitkamp, in: J.W. Ward (Ed.), Hydrocracking and Hydrotreating, in: ACS Symposium Series, Vol. 20, Am. Chem. Society, Washington, DC, 1975, pp. 1–27.
[32] J. Weitkamp, Erdoel, Kohle, Erdgas, Petrochem. 31 (1978) 13–22.
[33] F. Alvarez, F.R. Ribeiro, G. Perot, C. Thomazeau, M. Guisnet, J. Catal. 162 (1996) 179–189.
[34] G.F. Froment, Catal. Today 1 (1987) 455–473.
[35] G. Martens, G.F. Froment, Stud. Surf. Sci. Catal. 122 (1999) 333–340.
[36] G.G. Martens, G.B. Marin, J.A. Martens, P.A. Jacobs, B.V. Baron, J. Catal. 195 (2000) 253–267.
[37] J.W. Thybaut, G.B. Marin, G.V. Baron, P.A. Jacobs, J.A. Martens, J. Catal. 202 (2001) 324–339.
[38] J.F.M. Denayer, J.A. Martens, P.A. Jacobs, J.W. Thybaut, G.B. Marin, G.V. Baron, Appl. Catal. A 246 (2003) 17–28.
[39] J.A. Martens, P.A. Jacobs, in: J.B. Moffat (Ed.), Theoretical Aspects of Heterogeneous Catalysis, Van Nostrand Reinhold, New York, 1990, pp. 52–109.
[40] T.F. Degnan, C.R. Kennedy, AIChE J. 39 (1993) 607–614.
[41] M.M. Olken, J.M. Garces, in: R. von Ballmoos, J.B. Higgins, M.M.J. Treacy (Eds.), Proceedings from the Ninth International Zeolite Conference, Vol. 2, Butterworth–Heinemann, Boston, 1993, pp. 559–566.
[42] J.F. Denayer, G.V. Baron, G. Vanbutsele, P.A. Jacobs, J.A. Martens, J. Catal. 190 (2000) 469–473.
[43] J.F. Denayer, B. de Jonckheere, M. Hloch, G.B. Marin, G. Vanbutsele, J.A. Martens, G.V. Baron, J. Catal. 210 (2002) 445–452.
[44] J.F. Denayer, G.V. Baron, W. Souverijns, J.A. Martens, P.A. Jacobs, Ind. Eng. Chem. Res. 36 (1997) 3242–3247.
[45] J.A. Martens, P.A. Jacobs, J. Mol. Catal. 78 (1993) L47–L52.
[46] E.J.P. Feijen, J.A. Martens, P.A. Jacobs, Stud. Surf. Sci. Catal. 101 (1996) 721–729.
[47] J.A. Martens, J. Perez-Pariente, P.A. Jacobs, Acta Phys. Chem. 31 (1985) 487–495.